







## Effect of hydrostatic pressure on the quantum paraelectric state of dipolar coupled water molecular network

Y. T. Chan <sup>\*</sup>, E. Uykur , M. A. Belyanchikov, and M. Dressel <sup>†</sup>  
*1. Physikalisches Institut, Universität Stuttgart, 70569 Stuttgart, Germany*

V. A. Abalmasov   
*Institute of Automation and Electrometry SB RAS, 630090 Novosibirsk, Russia*

V. Thomas  
*Institute of Geology and Mineralogy, Russian Academy of Sciences, 630090 Novosibirsk, Russia*

E. S. Zhukova  and B. Gorshunov   
*Center for Photonics and 2D Materials, Moscow Institute of Physics and Technology, 141701 Dolgoprudny, Moscow Region, Russia*



(Received 6 April 2022; accepted 13 May 2022; published 13 June 2022)

We measure the real part  $\epsilon'$  of the dielectric permittivity of beryl crystals with heavy water molecules  $D_2O$  confined in nanosized cages formed by an ionic crystal lattice. The experiments are performed at a frequency of 1 MHz in the temperature interval from 300 down to 4 K under different hydrostatic pressures up to  $P = 6.3$  GPa. At high temperatures, a Curie-Weiss-like increase of  $\epsilon'(T)$  is observed upon cooling. Application of pressure leads to flattening of  $\epsilon'(T)$  at low temperatures due to quantum effects, i.e., tunneling of deuterium atoms in the hexagonal localizing potential. Analyzing the temperature behavior of  $\epsilon'$  with the Barrett expression allows us to obtain pressure dependencies of the quantum temperature  $T_1$ , the Curie-Weiss temperature  $T_C$ , and the Barrett constant  $C$ . The increase of  $T_1$  observed up to 4 GPa is associated with an enhanced azimuthal tunneling of the confined water molecules through the barriers of the potential. For  $P > 4$  GPa,  $T_1(P)$  levels off since the barriers disappear. Any further pressure increase does not affect the tunneling rate because of the absence of a barrier. The behavior is modeled by solving the Schrödinger equation for the water molecule in the azimuthal potential numerically. Small negative values of  $T_C \approx -10$  K obtained for  $P < 4$  GPa indicate the antiferroelectric ordering tendency of the water dipoles localized in the crystalline nanochannels. For higher pressure, a strong decrease of  $T_C$  toward negative values is observed that would correspond to the enhanced interdipole coupling strength, which is however hard to explain in the present case, and thus calls for additional theoretical and experimental studies.

DOI: [10.1103/PhysRevResearch.4.023205](https://doi.org/10.1103/PhysRevResearch.4.023205)

### I. INTRODUCTION

Incipient ferroelectrics provide a unique platform for studying quantum states of matter. In these materials, also named quantum paraelectrics, upon lowering the temperature, quantum fluctuations begin to prevail over thermally driven fluctuations of the order parameter and the dipole interaction energy. As a result, no long-range ordering of electric dipoles occurs. Physical properties of the resulting sea of interacting dipoles are then fully determined by quantum phenomena. Canonical examples of incipient ferroelectrics are strontium

titanate  $SrTiO_3$  [1] and potassium tantalate  $KTaO_3$  [2]. Due to quantum fluctuations, both compounds show no phase transition into an ordered state down to the lowest temperatures measured [3–5]. The crossover between classical and quantum regimes can be distinctly documented by measuring the temperature dependence of the low-frequency dielectric constant  $\epsilon'(T)$ , i.e., the real part of the complex dielectric permittivity  $\epsilon^* = \epsilon' + i\epsilon''$ . At high temperatures, it follows the Curie-Weiss dependence:

$$\epsilon' = \epsilon_\infty + \frac{C}{T - T_C}, \quad (1)$$

(here,  $C$  is the Curie constant,  $T_C$  the Curie temperature, and  $\epsilon_\infty$  is the high-temperature dielectric constant) but shows strong deviations around a specific temperature  $T_1$ , turning into a plateau that extends down to the lowest accessible temperatures. The temperature  $T_1$  is called the quantum temperature and sets the scale for the quantum fluctuations strength. The Barrett expression is commonly used to describe the behavior of the permittivity in the entire temperature

<sup>\*</sup>yuk-tai.chan@pi1.physik.uni-stuttgart.de

<sup>†</sup>Corresponding author: dressel@pi1.physik.uni-stuttgart.de

Published by the American Physical Society under the terms of the [Creative Commons Attribution 4.0 International](https://creativecommons.org/licenses/by/4.0/) license. Further distribution of this work must maintain attribution to the author(s) and the published article's title, journal citation, and DOI.

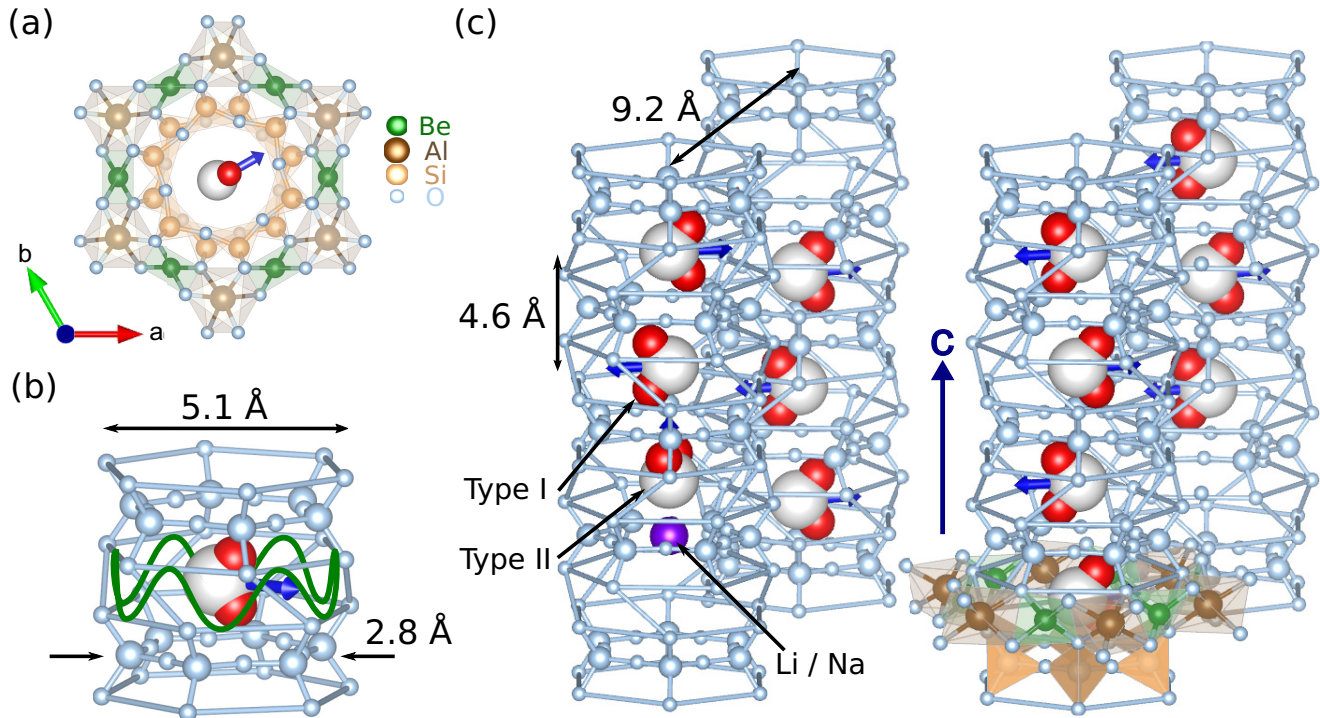


FIG. 1. (a) Beryl ( $\text{Be}_3\text{Al}_2\text{Si}_6\text{O}_{18}$ ) structure viewed along the  $c$  axis. Honeycomb six-membered Be, Al, and  $\text{SiO}_4$  tetrahedra enclose a water molecule (oxygen is gray, deuterium is red). The color coding of the atoms is given through the legend. The blue arrow indicates the dipole moment of the water molecule. (b) Separated water molecule within the ionic cage. The cage is in diameter of 5.1 Å with narrow bottlenecks of 2.8 Å. The water molecule encaged is subjected to a six-well localizing potential (green belt). (c) Schematic view of water molecules in nanosized cages of the hexagonal beryl crystal lattice. Cages are organized in channels aligned along the crystallographic  $c$  axis. Characteristic sizes are shown: interchannel distance (9.2 Å) and intercage distance along the channel (4.6 Å). Hydrogen bonding between water molecules is negated, and only dipole-dipole interaction is present.

interval [6]:

$$\epsilon' = \epsilon_\infty + \frac{C}{\frac{T_1}{2} \coth \frac{T_1}{2T} - T_C}. \quad (2)$$

The overall variation of the dielectric permittivity is directly linked to the dynamics of the low-energy transverse excitation of an optical phonon mode, the so-called ferroelectric soft mode. In the classical regime, the soft-mode frequency  $\nu_0$  and dielectric strength  $\Delta\epsilon$  follow the Cochran law [7],  $\nu_0 \propto (T - T_C)^{1/2}$ , and the Curie-Weiss law, expressed in Eq. (1), respectively. Below  $T_1$ , both parameters  $\Delta\epsilon$  and  $\nu_0$  level off and do not vary with temperature, meaning that the mode does not soften completely, and no phase transition occurs [8]. The nature of fundamental phenomena that determine qualitative changes in the behavior of the soft mode, i.e., of collective vibrations of the crystal lattice in incipient ferroelectrics when they enter the quantum regime, has been under intensive scrutiny for decades. Recently, the diversity of quantum phenomena in incipient ferroelectrics has been even enriched with quantum critical effects (see Ref. [9] and references therein) that have been discovered not only in the long-known  $\text{SrTiO}_3$  and  $\text{KTaO}_3$  [10,11] but also in other members of the family, e.g., the M-type hexaferrites [12,13], ferroelectric relaxors [14], and organic charge-transfer complexes [15–19].

Studies of quantum behavior and quantum-critical phenomena in ensembles of interacting electric dipoles are at the

cutting edge of today's condensed matter physics, especially given that the origin of the quantum criticality in electric systems based on Coulomb interactions should be strikingly different from that in magnetic compounds [9,10,20,21] where the quantum critical phenomena are determined by the spin degrees of freedom and have been the subject of numerous and detailed studies for many years [22]. Here, we investigate another type of quantum paraelectrics that differs from those described above in the way that the electric dipoles are not formed by displaced ions of the crystal lattice, as in conventional quantum paraelectrics, but are constituted by polar molecules bearing frozen-in electric dipoles. Ferroelectrics of this type were predicted in Ref. [23] where the ordered phase was described as composed of polar molecules sitting inside  $\text{C}_{60}$  cages. Similar materials of this sort were experimentally introduced [24] in the form of dielectric crystal of beryl ( $\text{Be}_3\text{Al}_2\text{Si}_6\text{O}_{18}$ ) and cordierite [ $(\text{Mg,Fe})_2\text{Al}_4\text{Si}_5\text{O}_{18}$ ], and those have subsequently been studied intensively [25–32].

Beryl crystallizes in a honeycomb structure (space group  $P6/mcc$ ) consisting of stacked six-membered rings of  $\text{SiO}_4$  tetrahedra, as depicted in Fig. 1. The latter leave relatively large open channels oriented parallel to the crystallographic  $c$  axis [33]. Along this axis, the channels contain bottlenecks of  $\sim 2.8$  Å alternating with slightly larger cages of 5.1 Å in diameter, into which separate polar water molecules (the dipole moment of an  $\text{H}_2\text{O}$  molecule is  $\sim 1.85$  Debye) can enter during crystal growth. The  $\text{H}_2\text{O}$  molecules occur in two

distinct orientations: either the two protons are aligned parallel to the  $c$  axis and the electric dipole points perpendicular to the  $c$  direction (type I), or the dipole moment points parallel to the  $c$  axis (type II; Fig. 1) [34,35]. With intercache distances of 5–9 Å (i.e., the distance between water molecules), the H<sub>2</sub>O molecules do not experience short-range hydrogen bonding but are subject to a longer-range dipole-dipole interaction. Being only weakly coupled to surrounding ions, type-I molecules are almost free to rotate around the  $c$  axis. One thus obtains an ideal playground for the studies of classical and quantum phenomena in a system of interacting point dipoles that qualitatively differs from conventional crystal lattice ferroelectrics and quantum paraelectrics.

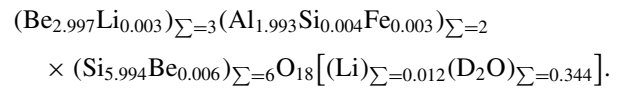
In previous radiofrequency and terahertz studies of hydrous beryl crystals [28], a terahertz ferroelectric soft mode was discovered; it was proven to be of nonphononic origin but associated exclusively with the response of coupled H<sub>2</sub>O dipoles. The temperature evolution of the soft mode caused a Curie-Weiss temperature behavior of the quasistatic permittivity of this dipolar network; however, no phase transition into the ordered phase has been observed. Below ~20 K and down to 300 mK, the permittivity saturates, signifying the suppression of a transition due to quantum tunneling of water molecular protons within the six-well localizing potential (Fig. 1). The strength and frequency of the terahertz soft mode show a similar leveling off below ~20 K. Modeling this behavior by the Barrett expression [Eq. (2)] allows the determination of characteristic temperatures, such as  $T_1 = 20$  K and  $T_C = -20$  K. It is also found that, in the quantum paraelectric regime, the water molecular ensemble displays clear signatures of quantum critical behavior [36]. The aim of this paper is to explore whether hydrostatic pressure can tune the water dipolar system toward a phase transition. Compression of the beryl crystal lattice brings the water dipoles closer together and thus enhances the dipole-dipole coupling. This might even overpower the other effect of proton delocalization due to tunneling. The idea was also inspired by reports where the application of pressure or strains effectively tunes the phonon system of traditional crystal lattice incipient ferroelectrics (see, e.g., Refs. [8,37–40] and references therein). To diminish the role of tunneling effects and make the water molecular system more prone to phase transition [30], we replace water protons with deuterium by synthesizing beryl crystals with nanoconfined heavy water molecules D<sub>2</sub>O.

## II. EXPERIMENTAL DETAILS

### A. Crystal growth

Beryl crystals were synthesized from oxides, using a complex acidic lithium-fluoride mineralizer [41,42] in sealed gold ampoules with a volume of ~60 mL placed in stainless-steel laboratory autoclaves at a temperature  $T \approx 600$  °C and pressure  $P \approx 1.5$  kbar. The volumes of the ampoule and autoclave were filled with D<sub>2</sub>O (the admixture of H<sub>2</sub>O did not exceed 0.1 wt. %). The grown crystal is characterized by its chemical composition averaged over the entire overgrown layer; we receive in wt. %: SiO<sub>2</sub>—66.18, Al<sub>2</sub>O<sub>3</sub>—18.66, BeO—13.80, Fe<sub>2</sub>O<sub>3</sub>—0.05, oxides of other 3d elements <0.01, Li<sub>2</sub>O—0.04, oxides of other alkaline elements <0.01, loss on

ignition (LOI)—1.14, yielding a total of 99.87 [43]. Assuming all LOIs are attributed to heavy water and following the recommendations presented in Ref. [44], the results can be recalculated into the following crystal chemical formula:



Recently, Belyanchikov *et al.* [43] found a correlation between lithium ions and some water molecules entering channel positions in the beryl structure: When the Li<sup>+</sup> is incorporated in the bottleneck of the channel, the two adjacent cages (above and below the bottleneck) are filled by water molecules whose dipole moments are parallel to the crystallographic  $c$  axis (the so-called water type II). This implies a certain distribution of the D<sub>2</sub>O molecules in beryl: only ~7% are D<sub>2</sub>O-II, while 93% are D<sub>2</sub>O-I.

### B. Radiofrequency measurements under hydrostatic pressure

In our experiments, the high-pressure environment was achieved by commercial diamond anvil cells (Almas Easy-Lab). The cell employs diamonds with 600 μm culets and a pre-indented CuBe gasket of 100 μm thickness. A 250 μm sample hole was machined by electric discharge at the center of the gasket. The beryl crystals were cut into 100 by 100 μm plates with a thickness of 70 μm using diamond styli (Agate Products); where the crystallographic  $c$  axis falls within the sample plane.

Since the contacts were placed on front and rear faces, the dielectric measurements are performed with the applied electric field in the  $ab$  plane. It is in this geometry that the quantum paraelectricity of the ensemble of nanoconfined water molecules was observed previously [28]. Quasi-four-probe dielectric measurements were performed with the help of an impedance analyzer (Agilent 4294A). The metallic contacts were made with silver paste (Plano G3303B) and gold wires of 15 μm diameter were used for voltage supply. Daphne oil 7474 was filled as the hydrostatic medium. The pressure was applied by manually tightening screws, with the help of a torque wrench. The real *in situ* pressure was determined by ruby fluorescence. The pressure cell could be cooled down to a base temperature of 4 K in a custom-made helium-flow cryostat.

### C. Monte Carlo simulations

The Metropolis algorithm was used to model the behavior of the dipole system at different temperatures. The dominant dipole-dipole interaction is given by the Hamiltonian:

$$H = (8\pi\epsilon_r\epsilon_0)^{-1} \sum_{ij} r_{ij}^{-3} [p_i p_j - 3(p_i n_{ij})(p_j n_{ij})]. \quad (3)$$

Here,  $\epsilon_0$  is the vacuum permittivity,  $\epsilon_r$  is the high-frequency relative dielectric constant due to electrons,  $r_{ij}$  is the distance between two dipoles  $p_i$  and  $p_j$ , and  $n_{ij}$  is the normal vector between them. Six dipole orientations were allowed, in contrast to previously modeled water molecules in cordierite, where there were only four possible orientations [45]. The presented results were obtained for a sample with 16 lattice sites along each axis (a total of 4096 sites) and a 30% dipole filling factor

with  $N = 1229$  dipoles in total. Free boundary conditions were applied. The dielectric susceptibility  $\chi = \epsilon' - 1$  along each axis  $\alpha$  was calculated from fluctuations of the average dipole  $p_\alpha = N^{-1} \sum_i^N p_i^\alpha$  as

$$\chi_\alpha = \frac{N p_0^2}{v_d \epsilon_0 k_B T} (\langle p_\alpha^2 \rangle - \langle p_\alpha \rangle^2). \quad (4)$$

Here,  $N$  is the number of dipoles in a simulation,  $p_0 = 1.85$  D is the dipole moment of a water molecule,  $v_d$  is the volume per dipole, and  $k_B$  is the Boltzmann constant. For each temperature  $T$ , the number of Monte Carlo steps per spin in the simulation was 11 000 (the first 1000 were attributed to thermalization). The results were averaged over 15 samples with different randomly generated dipole site configurations.

### III. RESULTS, ANALYSIS, AND DISCUSSION

Figure 2 depicts the water molecule dipole configuration in the  $ab$  and  $bc$  planes obtained from Monte Carlo simulation at zero temperature. Within the  $ab$  plane, no long-range order is developed given the presence of vacancies and the degenerate ground states of dipoles. Ferroelectric alignments are favored for adjacent dipoles, although exceptions can also be seen since the dipole interactions along the  $c$  axis are much stronger due to the smaller interdipole distance. Meanwhile, along the channels, the water molecules tend to form clusters with molecular dipole moments arranged antiferroelectrically (AFE).

The dielectric susceptibility  $\chi$  of water dipoles is also obtained from our Monte Carlo simulation, and the results are plotted in Fig. 3 together with the experimental data. The simulated  $\chi$  is deviated from the experimental result by a factor of  $\alpha = 2.5$ , and both data fit almost perfectly, especially at low temperatures, including a distinct kink at 20 K. (Note that the kink disappears for  $P > 4$  GPa.) We can attribute the discrepancy between experiment and simulation to the approximation included in the Monte Carlo simulations, where the dipoles were assumed to have only six fixed orientations, not considering the possible dipole tunneling and rotation in excited states. Use of the Curie-Weiss expression to fit the data provides negative  $T_C$  of approximately  $-10$  K, which is close to the values of  $T_C = -20$  K obtained in Ref. [28]. Drawing an analogy with the conventional crystal-lattice ferroelectrics, the negative  $T_C$  is pointing to an AFE type of dipole interaction.

In conventional AFEs, negative critical temperatures are usually obtained from infrared/terahertz spectroscopic measurements partially softened at the Brillouin zone center (at zero wave vector,  $k = 0$ ) transverse phonon branch. This behavior reflects the critical softening of the same phonon branch at the Brillouin zone boundary ( $k \neq 0$ ) where the bare soft mode develops, leading to the AFE phase transition at the critical temperature  $T_C$ . The presence of a soft mode in the form of a zero wave vector excitation in the terahertz spectra of hydrous beryl and its AFE-like contribution to the dielectric permittivity resulting in negative  $T_C$  can be explained by a certain friability of AFE ordered dipoles in the beryl channels that can couple to the spatially uniform ( $k = 0$ ) electric field.

Figure 4 presents temperature dependencies of the real part of the dielectric permittivity of hydrous beryl crystal measured

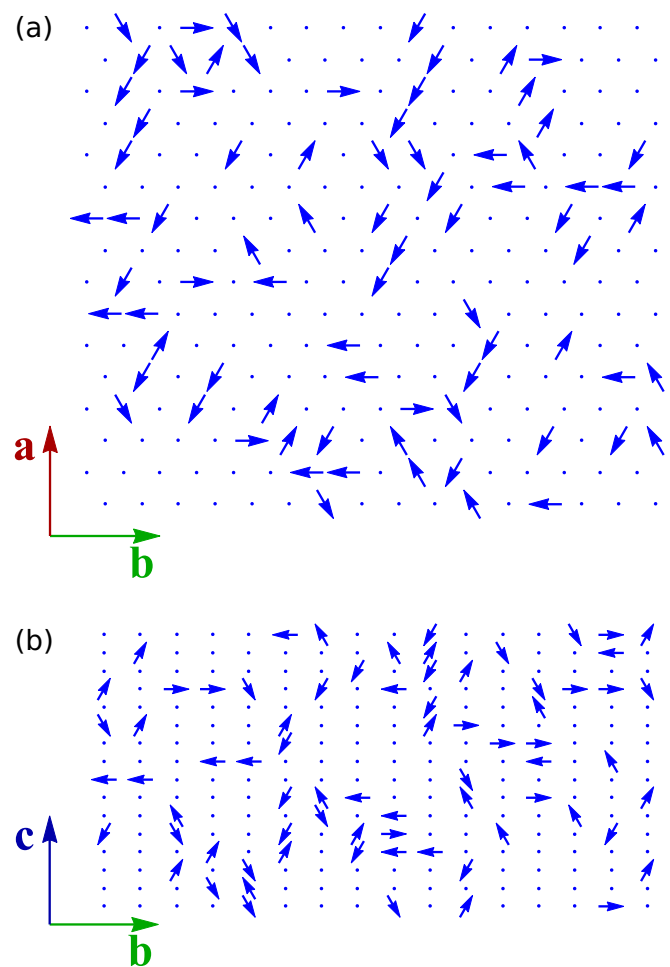


FIG. 2. Water molecule dipole configuration in (a) the  $ab$  plane and (b) the  $bc$  plane in beryl at zero temperature obtained by Monte Carlo simulation. (a) In the  $ab$  plane, the ferroelectric alignment is favored between adjacent water dipoles, but exceptions can be found, and no long-range order is developed. (b) The water dipoles have a zero component along the  $c$  axis. The vertical component of the dipole in this figure is the component in the  $a$  axis, such that the spatial configuration, in the  $bc$  plane, of the orientation of the dipole in the  $ab$  plane is displayed. We see the perfect antiferroelectric order along the  $c$  axis for the nearest dipoles.

at a frequency of 1 MHz under various pressures. Ambient pressure experiments on dehydrated samples obtained by heating them up to  $1000^\circ\text{C}$  and keeping them in a vacuum for a period of  $\sim 24$  h have shown that the observed strong temperature changes of permittivity are caused exclusively by the response of water molecules [28]. The lowest-temperature permittivity ( $< 20$ – $30$  K) is seen to be very sensitive to the application of pressure and decreases from ambient pressure values of  $\epsilon'(4\text{ K}) \approx 47$  to  $\sim 16$  at  $P = 6.3$  GPa. It is also seen that hydrostatic pressure does not induce any feature that could be associated with a ferroelectric or AFE phase transition, e.g., a characteristic peak in the temperature dependence of  $\epsilon'(T)$ . Instead, the effect of pressure results in gradual extension of the quantum paraelectric temperature range to higher temperatures, i.e., the temperature interval where  $\epsilon'(T)$  tends to saturation. Note that the low-temperature plateaus in

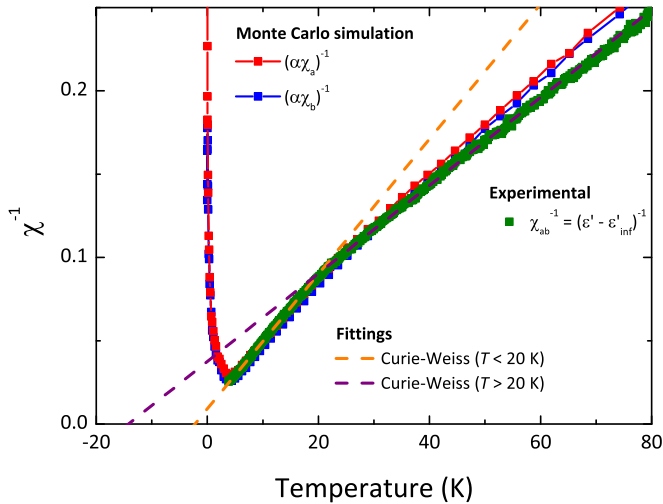


FIG. 3. Inverse dielectric susceptibility  $\chi^{-1}$  of water molecule dipoles in the  $ab$  plane of beryl. Lines and symbols correspond to  $\chi$  with the electric field polarization directed along  $a$  (red) and  $b$  (blue) Cartesian axes, respectively, obtained by Monte Carlo simulations. Experimental  $\chi$  (green square) is also extracted from  $\epsilon'$  by subtracting the high-temperature limit  $\chi = \epsilon' - \epsilon'_{\infty}$ . The simulated  $\chi$  will match with the experiment data by multiplying by a factor of  $\alpha = 2.5$ . The discrepancy is due to approximation in the model. The strong growth of  $\chi^{-1}$  below  $\approx 5$  K is because of the absence of quantum effects in Monte Carlo simulations. Dashed lines are extrapolations of Curie-Weiss fitting above (purple) and below (orange) the kink feature at 20 K. Both extrapolations project a negative  $T_C$ .

the  $\epsilon'(T)$  curves do not reveal any signs of shallow maxima that could indicate quantum critical phenomena [10,36].

The observed features in the temperature-pressure behavior of the permittivity are qualitatively like those obtained for strontium titanate (see Ref. [40], for instance). However, the underlying physics is completely different for the two systems: While in  $\text{SrTiO}_3$  the dielectric response is determined by the soft low-energy transverse phonon branch, the terahertz ferroelectric soft mode in hydrated beryl has its origin in the collective dynamics of interacting water dipoles [28,46].

Since the tunneling rate of a particle in a two-well potential depends exponentially on the width and the height of the barrier, we associate the aforementioned pressure-induced growth of the role of quantum effects and corresponding suppression of the phase transition with an enhanced quantum tunneling of the heavy water deuterium atoms within the localizing hexagonal potential, in full analogy to the tunneling of  $\text{H}_2\text{O}$  protons in beryl previously observed in spectroscopic experiments with hydrated beryl [27,28].

To get further insight into the pressure-induced changes of the dipole behavior, we performed least-square fits in the temperature variation of susceptibility, see Fig. 3. Because of the distinct kink feature, two temperature ranges, 4–20 K and 20–50 K, were chosen and fitted by the Barrett [Eq. (2), solid lines in Fig. 4] and Curie-Weiss [Eq. (1)] expressions, respectively. The obtained pressure dependencies of the quantum temperature  $T_1$ , the critical temperature  $T_C$ , and the constant  $C$  are plotted in Fig. 5. Here,  $T_C$  maintains its value of near  $-10$  K

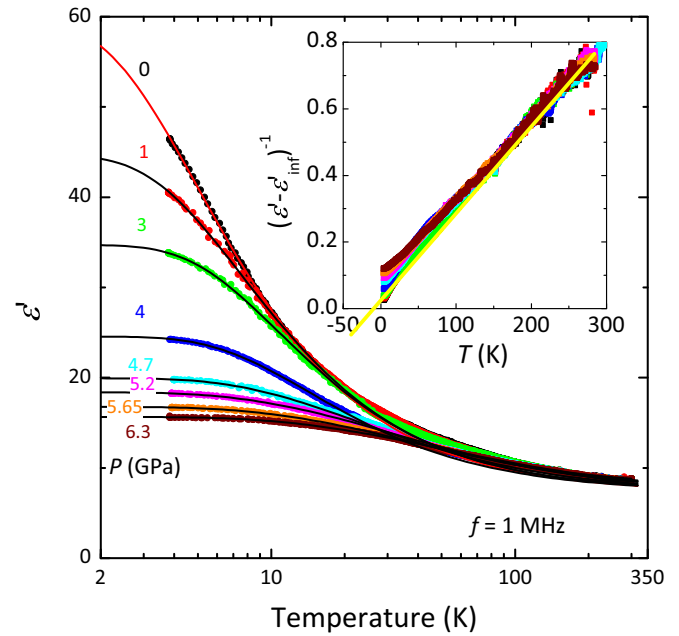


FIG. 4. Temperature dependencies of the real part of the permittivity  $\epsilon'$  of beryl crystal filled with heavy water molecules confined inside nanosized cages within the crystal lattice. The measurements are performed at a frequency of 1 MHz and at different hydrostatic pressures as indicated. Solid lines show results of least-square fits according to the Barrett expression in Eq. (2), as described in the text. The inset presents the corresponding dependencies of the inverse permittivity  $(\epsilon' - \epsilon'_{\infty})^{-1}$ , where  $\epsilon'_{\infty} \approx 7.3$  is the high-temperature dielectric constant independent of pressure. The colors in the inset correspond to those in the main panel. Straight line extrapolation toward zero values of  $(\epsilon' - \epsilon'_{\infty})^{-1}$  indicates negative critical temperature  $T_C \approx -10$  K.

at pressures up to 4 GPa, indicating a persistent AFE water molecule dipole interaction, and it is in perfect agreement with the Monte Carlo results (see Fig. 2). Rather unexpectedly, we observe a strong change in  $T_C$  toward large negative values for pressures above  $\approx 4$  GPa while, at the same time,  $C$  increases. The increase of negative  $T_C$  could be seen as an indication that the dipole-dipole interaction rises in strength; this, however, is very unlikely because the dipole separation changes only slightly under pressure. The crystal volume of beryl is reduced by only  $\sim 4\%$  at the highest pressure of  $\sim 6.3$  GPa obtained in our experiments [47]; this corresponds to a very small change in distance  $r$  between water molecules. Since the dipole-dipole interaction strength is proportional to  $r^{-3}$ , it increases not more than 4% with pressure of 6.3 GPa. An increase of  $T_C$  might also be caused by reorientation of water dipoles along the  $c$  axis as the potential barrier along the polar angle disappears at high pressure. Indeed, due to the anisotropy of the electric dipolar interaction, the coupling strength for collinear dipoles is twice as large. However, this does not provide an explanation of the observed increase of  $C$ . Since  $C$  is proportional to the dipole concentration, its growth at  $P > 4$  GPa could be connected to the pressure-induced hydration of beryl crystals, as has been reported [48], where a cordierite crystal was pressurized  $> 4$  GPa in aqueous medium. This would also explain the increase in the average

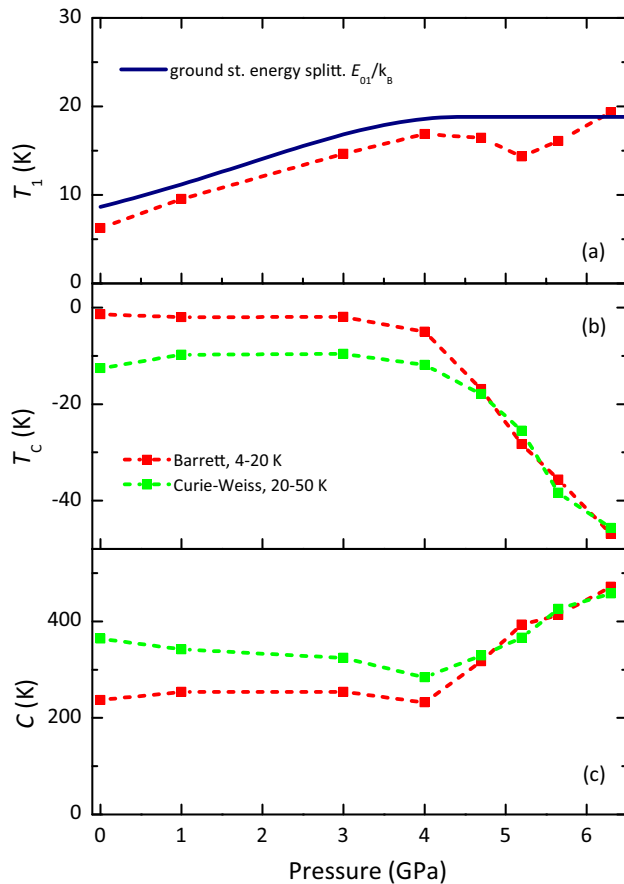


FIG. 5. Dependence on hydrostatic pressure of (a) quantum temperature  $T_1$ , (b) Curie-Weiss temperature  $T_C$ , and (c) Barrett constant  $C$  obtained by fitting the experimental data presented in Fig. 4 with the Barrett expression [Eq. (2)] in the temperature range 4–20 K and with the Curie-Weiss expression [Eq. (1)] in the temperature range 20–50 K. Dashed lines are guides for the eye. Dark blue solid line in (a) corresponds to the water molecule ground state energy splitting in the azimuthal potential (see text).

dipole interaction strength and  $T_C$  as the average distance between dipoles becomes smaller upon hydration. We feel, however, this line of argument is very unlikely because the pressure medium used in our experiment (Daphne oil) does not contain any water. To clarify and explain these unusual observations, further experimental and theoretical studies of  $T_C$  and  $C$  under pressure are needed.

We now turn to the pressure dependence of the quantum temperature  $T_1$ . We relate its increase with pressure up to  $\sim 4$  GPa [Fig. 5(a)] with an enhanced rate of quantum tunneling of deuterium atoms, caused by a suppression of the height and width of the potential barriers of the azimuthal hexagonal localizing potential. As seen in Fig. 5(a),  $T_1(P)$  saturates above  $\sim 4$  GPa. We suggest that this saturation is a sign of the disappearance of the barriers in the localizing potential, so that further increase of the pressure does not affect the tunneling rate because there are no barriers. Here, we should recall that the Barrett formula was initially obtained for a harmonic potential well with some anharmonic contributions [6], where  $T_1$  stands for the harmonic potential

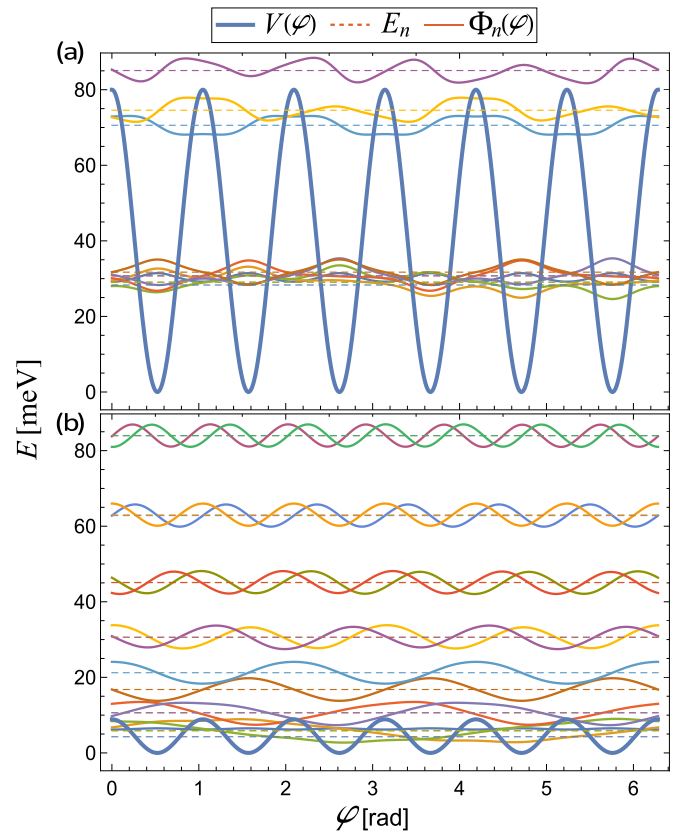


FIG. 6. Calculated (see text) energy levels of a water molecule in the azimuthal potential (a) at zero pressure and (b) at  $P = 4$  GPa. The thick blue curve is the potential energy, dashed lines are the energy levels, and solid lines are the corresponding wave functions.

frequency. Later, it was shown that the same formula describes the dielectric susceptibility of a particle in a double-well potential treated as a two-level system with  $T_1$  corresponding to the energy difference between the two tunnel-split states [49]. This means that, strictly speaking, Eq. (2) cannot be directly applied to the present case of a six-well potential: the water molecules in beryl are not localized in two wells, and hence, we do not have a two-level system. Nevertheless, fitting by the Barrett expression [Eq. (2)] gives us an effective value of the temperature due to quantum tunneling or anharmonic effects.

We assume that the quantum temperature  $T_1$  is related to the energy difference  $E_{01}$  between the ground and first excited states, i.e.,  $E_{01} \approx k_B T_1$  ( $k_B$  is the Boltzmann constant). We solve numerically the Schrödinger equation for the heavy water molecule with reduced mass  $m = m_O m_D / (m_O + m_D)$  (where  $m_O = 16$  and  $m_D = 4$  are oxygen and deuterium masses in amu), which is at a distance of  $d_{ab} = d \cos(\alpha_{\text{DOD}}/2)$  from the center of the nanopore in the  $ab$  plane; here,  $d = 0.96$  Å is the water molecule covalent bond length, and  $\alpha_{\text{DOD}} = 105^\circ$  is the angle between two covalent bonds. We approximate the azimuthal angle potential by  $V(\phi) = V_a [1 + \cos(6\phi)]/2$  (Fig. 6) with the amplitude  $V_a = V_0 \max[(1 - P/P_s), 0]$ , which is a linear function of pressure  $P$  and is zero above  $P_s = 4.5$  GPa. The obtained pressure dependence of the energy  $E_{01}$  is plotted as a solid line in Fig. 5(a), and it reproduces the experimentally obtained behavior quite well.

The saturation value of  $E_{01} = 1.64$  meV corresponds to the energy of the molecule free rotation around the  $c$  axis. The quantum temperature  $T_1 \approx 6$  K at zero pressure yields the estimation of  $V_0 = 80$  meV. This value is too high compared with the estimates of the localizing potential amplitude of  $\sim 1$  meV made in Ref. [30]. A lower value of  $V_0$  will be obtained if we assume that not only deuterium atoms but also oxygen atoms can tunnel during water molecule rotation, which will lead to a smaller potential barrier. This would be in accordance with mixed-type rotational-translational eigenmodes for a water molecule in beryl calculated in Ref. [30]. At the same time, the above potential parameters provide for the H<sub>2</sub>O molecule the zero-pressure value  $E_{01} \approx 2.1$  meV that is close to the energy of the soft mode of  $\approx 1.5$  meV measured in a neutron inelastic scattering experiment [27] and obtained by infrared spectroscopy [28] at low temperature. The density functional theory calculation in Ref. [27] also provides a high value for the potential barrier for water rotation around the  $c$  axis of  $\sim 176$  meV when the lattice is considered static and 48–56 meV when lattice vibrations are considered.

#### IV. CONCLUSIONS

Temperature- and pressure-dependent permittivity  $\epsilon'$  measurement at 1 MHz and Monte Carlo simulation were conducted on beryl crystal with nanoconfined quasifree water molecules. We could cover the temperature range from 4 to 300 K and apply hydrostatic pressure up to  $P = 6.3$  GPa. With increasing pressure, the low-temperature  $\epsilon'(T)$  progressively

flattens due to quantum tunneling of the heavy water, i.e., the orientation of the D<sub>2</sub>O dipole moment in the hexagonal localizing potential. The Barrett expression for  $\epsilon'(T)$  is used to obtain the pressure dependencies of the quantum temperature  $T_1$ , Curie-Weiss temperature  $T_C$ , and Barrett constant  $C$ . An increase of  $T_1(P)$  is observed up to  $\sim 4$  GPa followed by a leveling off at higher pressures. This behavior is associated with an enhanced azimuthal tunneling of confined water molecules through potential barriers of crystalline localizing potential that flattens at  $P > 4$  GPa, when a further increase of the pressure does not affect the tunneling rate because there are no barriers. Small negative values ( $T_C \approx -10$  K) obtained for  $P < 4$  GPa indicate the antiferroelectric ordering tendency of water dipoles localized in the nanochannels. The anomalous behavior of the Curie-Weiss temperature  $T_C$  observed at  $P > 4$  GPa (pronounced decrease toward negative values) and the Barrett constant  $C$  (strong growth) call for further theoretical and experimental studies.

#### ACKNOWLEDGMENTS

The authors thank M. Savinov and J. Petzelt for fruitful discussions. We acknowledge the exchange with M. Fyta and H.-P. Büchler and the financial support by the Deutsche Forschungsgemeinschaft via DR228/61-1. This paper was supported by the Ministry of Science and Higher Education of the Russian Federation (No. FSMG-2021-0005) and the Russian Foundation for Basic Research (Project No. 20-02-00314).

- 
- [1] V. V. Lemanov, Improper ferroelastic SrTiO<sub>3</sub> and what we know today about its properties, *Ferroelectrics* **265**, 1 (2002).
- [2] D. Rytz, U. T. Höchli, and H. Bilz, Dielectric susceptibility in quantum ferroelectrics, *Phys. Rev. B* **22**, 359 (1980).
- [3] K. A. Müller and H. Burkard, SrTiO<sub>3</sub>: an intrinsic quantum paraelectric below 4 K, *Phys. Rev. B* **19**, 3593 (1979).
- [4] O. E. Kvyatkovskii, Quantum effects in incipient and low-temperature ferroelectrics (a review), *Phys. Solid State* **43**, 1401 (2001).
- [5] M. E. Lines and A. M. Glass, *Principles and Applications of Ferroelectrics and Related Materials* (Oxford University Press, Oxford, 1977).
- [6] J. H. Barrett, Dielectric constant in perovskite type crystals, *Phys. Rev.* **86**, 118 (1952).
- [7] Y. Takagi and T. Shigenari, Characteristics of a generalized susceptibility for the analysis of lineshapes of Raman spectra, *J. Raman Spectrosc.* **10**, 158 (1981).
- [8] S. Kamba, Soft-mode spectroscopy of ferroelectrics and multiferroics: a review, *APL Mater.* **9**, 020704 (2021).
- [9] P. Chandra, G. G. Lonzarich, S. E. Rowley, and J. F. Scott, Prospects and applications near ferroelectric quantum phase transitions: a key issues review, *Rep. Prog. Phys.* **80**, 112502 (2017).
- [10] S. E. Rowley, L. J. Spalek, R. P. Smith, M. P. M. Dean, M. Itoh, J. F. Scott, G. G. Lonzarich, and S. S. Saxena, Ferroelectric quantum criticality, *Nat. Phys.* **10**, 367 (2014).
- [11] J. Hemberger, M. Nicklas, R. Viana, P. Lunkenheimer, A. Loidl, and R. Böhmer, Quantum paraelectric and induced ferroelectric states in SrTiO<sub>3</sub>, *J. Phys.: Condens. Matter* **8**, 4673 (1996).
- [12] S.-P. Shen, Y.-S. Chai, J.-Z. Cong, P.-J. Sun, J. Lu, L.-Q. Yan, S.-G. Wang, and Y. Sun, Magnetic-ion-induced displacive electric polarization in FeO<sub>5</sub> bipyramidal units of (Ba, Sr)Fe<sub>12</sub>O<sub>19</sub> hexaferrites, *Phys. Rev. B* **90**, 180404(R) (2014).
- [13] H. B. Cao, Z. Y. Zhao, M. Lee, E. S. Choi, M. A. McGuire, B. C. Sales, H. D. Zhou, J.-Q. Yan, and D. G. Mandrus, High pressure floating zone growth and structural properties of ferrimagnetic quantum paraelectric BaFe<sub>12</sub>O<sub>19</sub>, *APL Mater.* **3**, 062512 (2015).
- [14] R. M. Smith, J. Gardner, F. D. Morrison, S. E. Rowley, C. Ferraz, M. A. Carpenter, J. Chen, J. Hodgkinson, S. E. Dutton, and J. F. Scott, Quantum critical points in ferroelectric relaxors: stuffed tungsten bronze K<sub>3</sub>Li<sub>2</sub>Ta<sub>5</sub>O<sub>15</sub> and lead pyrochlore (Pb<sub>2</sub>Nb<sub>2</sub>O<sub>7</sub>), *Phys. Rev. Materials* **2**, 084409 (2018).
- [15] S. Horiuchi, Y. Okimoto, R. Kumai, and Y. Tokura, Quantum phase transition in organic charge-transfer complexes, *Science* **299**, 229 (2003).
- [16] F. Kagawa, N. Minami, S. Horiuchi, and Y. Tokura, Athermal domain-wall creep near a ferroelectric quantum critical point, *Nat. Commun.* **7**, 10675 (2016).
- [17] F. Kagawa, S. Horiuchi, and Y. Tokura, Quantum phenomena emerging near a ferroelectric critical point in a donor-acceptor organic charge-transfer complex, *Crystals* **7**, 106 (2017).
- [18] S. Tomić and M. Dressel, Ferroelectricity in molecular solids: a review of electrodynamic properties, *Rep. Prog. Phys.* **78**, 096501 (2015).

- [19] M. Dressel and S. Tomić, Molecular quantum materials: electronic phases and charge dynamics in two-dimensional organic solids, *Adv. Phys.* **69**, 1 (2020).
- [20] S. Rowley, R. Smith, M. Dean, L. Spalek, M. Sutherland, M. Saxena, P. Alireza, C. Ko, C. Liu, E. Pugh, S. Sebastian, and G. Lonzarich, Ferromagnetic and ferroelectric quantum phase transitions, *Phys. Stat. Sol. (b)* **247**, 469 (2010).
- [21] S.-P. Shen, J.-C. Wu, J.-D. Song, X.-F. Sun, Y.-F. Yang, Y.-S. Chai, D.-S. Shang, S.-G. Wang, J. F. Scott, and Y. Sun, Quantum electric-dipole liquid on a triangular lattice, *Nat. Commun.* **7**, 10569 (2016).
- [22] H. v. Löhneysen, A. Rosch, M. Vojta, and P. Wölfle, Fermi-liquid instabilities at magnetic quantum phase transitions, *Rev. Mod. Phys.* **79**, 1015 (2007).
- [23] J. Cioslowski and A. Nanayakkara, Endohedral Fullerites: A New Class of Ferroelectric Materials, *Phys. Rev. Lett.* **69**, 2871 (1992).
- [24] B. P. Gorshunov, E. S. Zhukova, V. I. Torgashev, G. S. S. V. V. Lebedev, R. K. Kremer, E. V. Pestrjakov, V. G. Thomas, D. A. Fursenko, and M. Dressel, Quantum behavior of water molecules confined to nanocavities in gemstones, *J. Phys. Chem. Lett.* **4**, 2015 (2013).
- [25] E. S. Zhukova, V. I. Torgashev, B. P. Gorshunov, G. S. S. V. V. Lebedev, R. K. Kremer, E. V. Pestrjakov, V. G. Thomas, D. A. Fursenko, A. S. Prokhorov, and M. Dressel, Vibrational states of a water molecule in a nano-cavity of beryl crystal lattice, *J. Chem. Phys.* **140**, 224317 (2014).
- [26] B. P. Gorshunov, E. S. Zhukova, V. I. Torgashev, E. A. Motovilova, V. V. Lebedev, A. S. Prokhorov, G. S. Shakhurov, R. K. Kremer, V. V. Uskov, E. V. Pestrjakov *et al.*, THz-IR spectroscopy of single H<sub>2</sub>O molecules confined in nanocage of beryl crystal lattice, *Phase Trans.* **87**, 966 (2014).
- [27] A. I. Kolesnikov, G. F. Reiter, N. Choudhury, T. R. Prisk, E. Mamontov, A. Podlesnyak, G. Ehlers, A. G. Seel, D. J. Wesolowski, and L. M. Anovitz, Quantum Tunneling of Water in Beryl: A New State of the Water Molecule, *Phys. Rev. Lett.* **116**, 167802 (2016).
- [28] B. P. Gorshunov, V. I. Torgashev, E. S. Zhukova, V. G. Thomas, M. A. Belyanchikov, C. Kadlec, F. Kadlec, M. Savinov, T. Ostapchuk, J. Petzelt *et al.*, Incipient ferroelectricity of water molecules confined to nano-channels of beryl, *Nat. Commun.* **7**, 12842 (2016).
- [29] Y. Finkelstein, R. Moreh, S. L. Shang, Y. Wang, and Z. K. Liu, Quantum behavior of water nano-confined in beryl, *J. Chem. Phys.* **146**, 124307 (2017).
- [30] M. A. Belyanchikov, E. S. Zhukova, S. Tretiak, A. Zhugayevych, M. Dressel, F. Uhlig, J. Smiatek, M. Fyta, V. G. Thomas, and B. P. Gorshunov, Vibrational states of nano-confined water molecules in beryl investigated by first-principles calculations and optical experiments, *Phys. Chem. Chem. Phys.* **19**, 30740 (2017).
- [31] A. I. Kolesnikov, L. M. Anovitz, F. C. Hawthorne, A. Podlesnyak, and G. K. Schenter, Effect of fine-tuning pore structures on the dynamics of confined water, *J. Chem. Phys.* **150**, 204706 (2019).
- [32] M. A. Belyanchikov, M. Savinov, Z. V. Bedran, P. Bednyakov, P. Proschek, J. Prokleska, V. A. Abalmasov, J. Petzelt, E. S. Zhukova, V. G. Thomas *et al.*, Dielectric ordering of water molecules arranged in a dipolar lattice, *Nat. Commun.* **11**, 3927 (2020).
- [33] G. Gibbs, D. Breck, and E. Meagher, Structural refinement of hydrous and anhydrous synthetic beryl, Al<sub>2</sub>(Be<sub>3</sub>Si<sub>6</sub>)O<sub>18</sub> and emerald, Al<sub>1.9</sub>Cr<sub>0.1</sub>(Be<sub>3</sub>Si<sub>6</sub>)O<sub>18</sub>, *Lithos* **1**, 275 (1968).
- [34] D. L. Wood and K. Nassau, The characterization of beryl and emerald by visible and infrared absorption spectroscopy, *Am. Mineral.* **53**, 777 (1968).
- [35] G. Artioli, R. Rinaldi, K. Stahl, and P. F. Zanazzi, Structure refinements of beryl by single-crystal neutron and x-ray diffraction, *Am. Mineral.* **78**, 762 (1993).
- [36] M. A. Belyanchikov, M. Savinov, P. Proschek, J. Prokleska, E. S. Zhukova, V. G. Thomas, Z. V. Bedran, F. Kadlec, S. Kamba, M. Dressel *et al.*, Fingerprints of critical phenomena in a quantum paraelectric ensemble of nanoconfined water molecules, *Nano Lett.* **22**, 3380 (2022).
- [37] G. A. Samara, Glasslike Behavior and Novel Pressure Effects in KTa<sub>1-x</sub>Nb<sub>x</sub>O<sub>3</sub>, *Phys. Rev. Lett.* **53**, 298 (1984).
- [38] G. A. Samara, Pressure-Induced Crossover from Long- to Short-Range Order in Compositionally Disordered Soft Mode Ferroelectrics, *Phys. Rev. Lett.* **77**, 314 (1996).
- [39] G. A. Samara, Pressure as a probe of the glassy properties of disordered ferroelectrics, antiferroelectrics and dielectrics, *Ferroelectrics* **117**, 347 (1991).
- [40] R. Wang, N. Sakamoto, and M. Itoh, Effects of pressure on the dielectric properties of SrTi<sub>18</sub>O<sub>3</sub> and SrTi<sub>16</sub>O<sub>3</sub> single crystals, *Phys. Rev. B* **62**, R3577 (2000).
- [41] A. Lebedev, A. Il'in, and V. Klyakhin, Hydrothermally grown beryls of gem quality (in Russian), Morphology and Phase Equilibria of Minerals, *Proceedings of the 13th General Meeting of the International Mineralogical Association, Varna* (Sofia, Bulgaria, 1982), Vol. 2, p. 403 (1986).
- [42] V. Thomas and V. Klyakhin, Specific features of incorporation of chromium in the beryl structure under hydrothermal conditions (experimental data), in *Mineral Forming in Endogenic Processes*, edited by N. V. Sobolev (Nauka, Novosibirsk, 1987), p. 60.
- [43] M. A. Belyanchikov, P. A. Abramov, A. L. Ragozin, D. A. Fursenko, B. P. Gorshunov, and V. G. Thomas, Distribution of D<sub>2</sub>O molecules of first and second types in hydrothermally grown beryl crystals, *Cryst. Growth Des.* **21**, 2283 (2021).
- [44] V. V. Bakakin and N. V. Belov, Crystal chemistry of beryl, *Geokhimiya (USSR)* **5** (1962).
- [45] V. A. Abalmasov, Dipole ordering of water molecules in cordierite: Monte Carlo simulations, *J. Phys.: Condens. Matter* **33**, 34LT01 (2021).
- [46] Y. Nakajima and S. Naya, Orientational phase transition and dynamic susceptibility of hindered-rotating dipolar system—a librator-rotator model, *J. Phys. Soc. Jpn.* **63**, 904 (1994).
- [47] D. Fan, J. Xu, Y. Kuang, X. Li, Y. Li, and H. Xie, Compressibility and equation of state of beryl (Be<sub>3</sub>Al<sub>2</sub>Si<sub>6</sub>O<sub>18</sub>) by using a diamond anvil cell and *in situ* synchrotron x-ray diffraction, *Phys. Chem. Minerals* **42**, 529 (2015).
- [48] A. Y. Likhacheva, S. V. Goryainov, and T. A. Bul'bak, An x-ray diffraction study of the pressure-induced hydration in cordierite at 4–5 GPa, *Am. Mineral.* **98**, 181 (2013).
- [49] R. Blinc and B. Žekš, *Soft Modes in Ferroelectrics and Antiferroelectrics*, Science Education and Future Human Needs Series (North-Holland, Amsterdam, 1974).